Results in Physics 10 (2018) 558–567

Contents lists available at ScienceDirect

Results in Physics

journal homepage: www.elsevier.com/locate/rinp

Corrosion inhibition of mild steel in HCl medium by S-benzyl-O, O'-bis(2-naphthyl)dithiophosphate with ultra-long lifespan

Chengduan Wang[a], Chuan Lai[a,b], Bin Xie[b,*], Xiaogang Guo[c], Dong Fu[a], Bin Li[a], Shasha Zhu[b]

[a] School of Chemistry and Chemical Engineering, Eastern Sichuan Sub-center of National Engineering Research Center for Municipal Wastewater Treatment and Reuse, School of Intelligent Manufacturing, Sichuan University of Arts and Science, Dazhou 635000, China

[b] School of Materials Science and Engineering, Material Corrosion and Protection Key Laboratory of Sichuan Province, Key Laboratories of Fine Chemicals and Surfactants in Sichuan Provincial Universities, Key Laboratory of Green Catalysis of Higher Education Institutes of Sichuan, Sichuan University of Science and Engineering, Zigong 643000, China

[c] College of Chemistry and Chemical Engineering, Yangtze Normal University, Chongqing 408100, China

ARTICLE INFO

Keywords:
O,O'-diaryldithiophosphates
Synthesis
Crystal structure
Corrosion inhibition
Ultra-long lifespan

ABSTRACT

Herein, the target compound of S-benzyl-O,O'-bis(2-naphthyl)dithiophosphate (SBOB) as corrosion inhibitor with ultra-long lifespan was successfully synthesized and characterized by elemental analysis, single crystal X-ray diffraction and spectroscopy involving FT-IR, ^{1}H, ^{13}C and ^{31}P NMR. Meanwhile, the inhibition performance and mechanism of SBOB for mild steel (MS) in HCl medium were combined to investigate by weight loss, potentiodynamic polarization, electrochemical impedance spectroscopy, scanning electron microscopy and quantum chemical calculation. The potentiodynamic polarization results indicate that SBOB is a mixed-type inhibitor. All experimental results are in good agreement and reveal that the corrosion inhibition increases with the concentration of SBOB. Weight loss results indicate that the inhibition efficiency decreases with HCl concentration and temperature increasing, but the corrosion inhibition performance of SBOB keeps almost unchanged after ultra-long storage time due to the formation of inhibitor film by the physisorption and chemisorption of SBOB on MS surface.

Introduction

Acid solutions, especially the different concentrations of hydrochloric acid solutions, are widely used in industry for cleaning, descaling, pickling, and oil well acidizing [1,2]. In fact, the corrosion phenomenon for various metals is especially prominent in these industries processes. More and more researchers have to admit that the problem has become a serious challenge to scientists and engineers. As a classical construction and engineering metal material, mild steel is widely used in a variety of chemical and petrochemical industries resulting from its excellent mechanical property, availability and low cost [3]. But the mild steels are easily serious corroded by different acid aggressive solutions. As a matter of fact, among various techniques to control and suppress mild steel corrosion, one of the most efficient methods is to use different inhibitors [4,5]. Therefore, to exploit new corrosion inhibitors using for mild steel in aggressive acid solutions are important not only in practical applications but also for academic value.

Up to now, organic compounds turn out to be a kind of effective corrosion inhibitors. For example, Xhanari [6] and Lamaka [7] summarized and reported that more than two hundred organic compounds can be used as inhibitors for magnesium, aluminium and their alloys corrosion. Furthermore, the amine derivative of 1,3,5-tris(4-aminophenoxy)benzene [8], 2-Pyridinecarbo-nitrile [9], acrylamide methyl ether [10], N-Methylol acrylamide [10], 1,2,3-ttriazole derivatives of (1-Benzyl-1H-1,2,3-triazole-4-yl) methanol [11] and (1-(pyridin-4-ylmethyl)-1H-1,2,3-triazole-4-yl)methanol [11], and imidazoline derivatives of 2-(2-trifluoromethyl-4,5-dihydro-imidazol-1-yl)-ethylamine [12] and 2-(2-trichloromethyl-4,5-dihydro-imidazol-1-yl)-ethylamine [12] also reported as the effective corrosion inhibitor in recent years.

Based on the relationships between inhibitors structure and their corrosion inhibition performance, the O,O'-diaryldithiophosphates and their derivatives maybe can act as the effective inhibitors because of the N, P and S atoms in the structures. The different O,O'-dialkyldi-thiophosphates diethyl ammonium as corrosion inhibitors has been reported in our previous works [13,14], but the derivatives of O,O'-diaryldithiophosphates as the excellent corrosion inhibitor with ultra-long lifespan has not been studied.

* Corresponding author at: No. 180 Xue Yuan Jie, Zi Gong 643000, China.
E-mail address: xiebinsuse@163.com (B. Xie).

https://doi.org/10.1016/j.rinp.2018.07.002
Received 5 June 2018; Received in revised form 4 July 2018; Accepted 5 July 2018
Available online 11 July 2018

Table 1
The composition of test specimens and working electrode (in wt.%).

Element	Mn	Si	C	P	S	Fe
Composition	0.419	0.268	0.165	< 0.015	< 0.011	Bal.

In order to develop more corrosion inhibitors, S-benzyl-O,O'-bis(2-naphthyl)dithiophosphate (SBOB) with ultra-long lifespan would be presented in this work. Meanwhile, different methods would be used to evaluate the performance of corrosion inhibition and clarify the inhibition mechanism by SBOB.

Materials and methods

Materials

All chemicals containing reagents and solvents involving P_2S_5 (phosphorus pentasulphide), 2-$C_{10}H_7OH$ (2-naphthol), $HNEt_2$ (diethylamine), CH_2Cl_2 (dichloromethane), $PhCH_2Br$ (benzyl bromide), $PhCH_3$ (toluene), CH_3COCH_3 (acetone) and HCl (hydrochloric acid, 37%) used to synthesize corrosion inhibitor and prepare the test solutions were analytically pure and purchased from Sinopharm Chemical Reagent Co., Ltd (China). The test specimens (2 × 25 × 50 mm, S = 28.0 cm^2) and working electrode (working area 0.785 cm^2) used to evaluate inhibition action that were fabricated by MS (mild steel) and the chemical compositions given in Table 1.

Moreover, the synthesized inhibitor would be confirmed by elemental analysis (1106), fourier transform infrared spectrometer (FT-IR, Nicolet-6700) and nuclear magnetic resonance (NMR, Brucker AV400). Meanwhile, crystal data were collected on a Bruker Smart Apex II CCD diffractomenter. Electrochemical tests were employed by electrochemical workstation (CHI 660D) using a Pt electrode and saturated calomel reference electrode (SCE) as the counter and reference electrode, respectively.

Synthesis of SBOB

For synthetic the corrosion inhibitor of S-benzyl-O,O'-bis(2-naphthyl)dithiophosphate (SBOB, (2-$C_{10}H_7O)_2P(S)SCH_2Ph$), the ammonium salt of (2-$C_{10}H_7O)_2P(S)SNH_2Et_2$, namely O,O'-bis (2-naphthyl) dithiophosphate diethyl ammonium, was synthesized by the reaction of P_2S_5, 2-$C_{10}H_7OH$ and $HNEt_2$ in toluene based on our previous reports [13,14]. Then, the target inhibitor of SBOB was synthesized by (2-$C_{10}H_7O)_2P(S)SNH_2Et_2$ and $PhCH_2Br$ in CH_2Cl_2 as solvent according to the detailed process described in references [15,16]. The synthetic route and corresponding chemical structures of (2-$C_{10}H_7O)_2P(S)SNH_2Et_2$ and target compound of SBOB are shown in Fig. 1.

Weight loss measurement

To evaluate the inhibition action of inhibitor, weight loss measurement was described in different literatures [17–19]. By using this method, the corrosion rate (v) and inhibition efficiency (η_W, %) were calculated from Eqs. (1) and (2), respectively. Where m_0 and m_i are the mass of the test specimen before and after corrosion, S = 28.0 cm^2, t is the immersion time, v_i and v_0 are corrosion rate of the MS specimen in HCl medium with and without different concentrations SBOB.

$$v_i = \frac{m_0 - m_i}{St} \tag{1}$$

$$\eta_W(\%) = \frac{v_0 - v_i}{v_0} \times 100\% \tag{2}$$

Potentiodynamic polarization measurement (Tafel)

According to this measurement, the potential sweep rate was 0.5 mV s^{-1}. Corrosion current density ($I_{c(i)}$) was determined from the intercept of extrapolated cathodic and anodic Tafel lines at the corrosion potential ($E_{c(i)}$). The inhibition efficiency (η_T, %) obtained by this method was calculated by Eq. (3) [20–22], where $I_{c(i)}$ and $I_{c(0)}$ are the corrosion current density values of MS corrosion in HCl medium with and without different concentrations SBOB.

$$\eta_T(\%) = \frac{I_{c(0)} - I_{c(i)}}{I_{c(0)}} \times 100\% \tag{3}$$

Electrochemical impedance spectroscopy (EIS)

Electrochemical impedance spectroscopy (EIS) was performed in frequency range of 100 kHz to 10 mHz using a sinusoidal AC perturbation with amplitude of 10 mV. Charge transfer resistance (R_{ct}) was

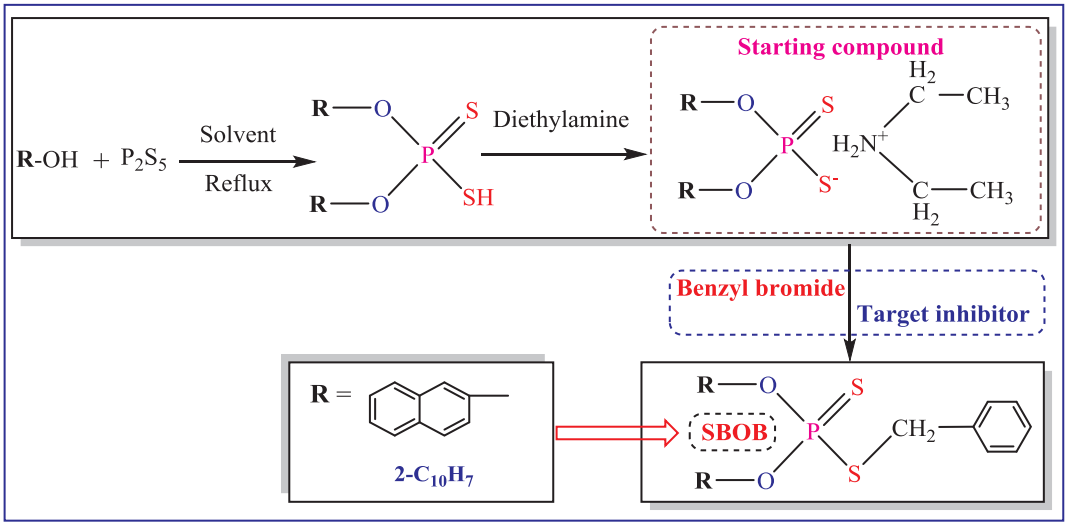

Fig. 1. Synthetic route of SBOB.

Table 2
The elemental analysis data of SBOB.

Molecular formula	Molecular weight	Anal. Calcd (%)			Anal. Found (%)		
		C	H	S	C	H	S
$C_{27}H_{21}O_2PS_2$	473	68.62	4.48	1.357	68.64	4.50	1.358

obtained from the diameter of semicircle by Nyquist plot. The corresponding inhibition efficiency (η_E, %) derived from this method was calculated by Eq. (4) [20–22], where $R_{ct(0)}$ and $R_{ct(i)}$ are the values of charge transfer resistance observed by MS corrosion in HCl medium in the absence and presence of different concentration of SBOB.

$$\eta_T(\%) = \frac{R_{ct(i)} - R_{ct(0)}}{R_{ct(i)}} \times 100\% \quad (4)$$

The working electrode was immersed in test solution at open circuit potential (OCP) for 30 min to be sufficient to attain a stable state before Tafel and EIS measurement. Meanwhile, all measurements containing weight loss, Tafel and EIS measurements were taken in the static test solutions.

Calculation details

The molecular structure of SBOB using to quantum chemical calculations was fully optimized by density functional theory (DFT) using B3LYP functional with 6–311 + + G (d, p) basis set [23,24]. The parameters of E_{HOMO}, E_{LUMO}, and ΔE ($\Delta E = E_{LUMO} - E_{HOMO}$) were obtained and calculated.

Scanning electron microscopy

The surface morphologies of MS samples before and after immersion in 1.0 M HCl at 303 K in the absence and presence of 40 mg L^{-1} and 100 mg L^{-1} SBOB for 2.0 h were examined by scanning electron microscopy (SEM, Tescan Vega III) at the points of interest.

Results and discussion

Characterization of SBOB

Elemental analysis, FT-IR and NMR

In order to confirm the molecular structure of the synthesized compound of SBOB, the elemental analysis, FT-IR, ^{1}H NMR, ^{13}C NMR and ^{31}P NMR were employed to analyze the inhibitor structural of SBOB. The elemental analysis results were listed in Table 2. The value of the calculated and observed data (Anal. Calcd. and Anal. Found, %) for SBOB is in good agreement and fit well with the SBOB structure presenting in Fig. 1. The FT-IR (Table 3 and Fig. 2) and NMR (^{1}H, ^{13}C and ^{31}P, see Table 4) results further confirmed the SBOB structure.

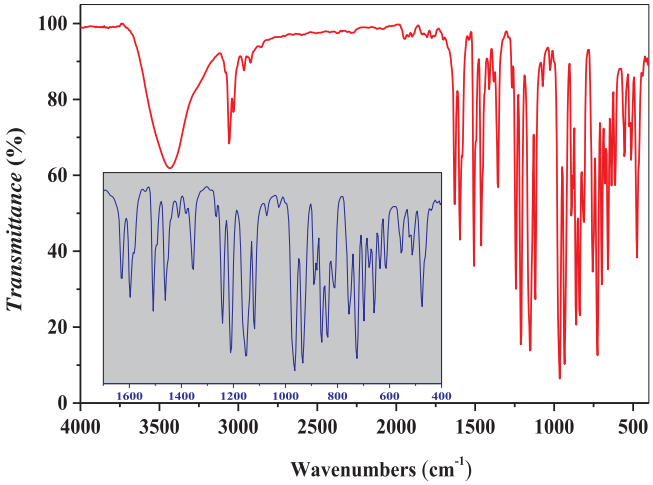

Fig. 2. The FT-IR spectra of SBOB.

Table 4
^{1}H, ^{13}C and ^{31}P NMR data of SBOB.

δ (ppm)		
^{1}H NMR	^{13}C NMR	^{31}P NMR
4.36 (d, *J* = 16.81 Hz, 2H, S*CH*$_2$), 7.31–7.72 (m, 5H, Ph-*H*), 7.51–7.93 (m, 14H, 2 (2-C$_{10}$*H*$_7$))	39.29 (*SCH*$_2$), 118.56, 118.60, 121.30, 125.80, 126.72, 127.85, 128.76, 129.16, 129.68, 131.36, 133.79, 136.49, 148.18(Ph-*C*, 2(2-*C*$_{10}$H$_7$))	90.21 (t, *J* = 16.81 Hz)

Crystal data, structure determination and analysis of SBOB

A colorless block single crystal with dimensions 0.34 × 0.30 × 0.26 mm^3 was selected and used to determine the structure of SBOB by single crystal X-ray diffraction. All the crystal data were collected and summarized in Table 5. The final cycle of refinement gave $(\Delta\rho)_{max}$ was 0.448 e $Å^{-3}$ and $(\Delta\rho)_{min}$ was −0.498 e $Å^{-3}$. (*CCDC 1818270*).

The molecular structure of SBOB is shown in Fig. 3. Meanwhile, the selected bond distances and bond angles of SBOB are listed in Table 6. It can be found that the compound of SBOB is crystallized in the monoclinicspace group $P2_1/c$. A distorted tetrahedral environment around phosphorus atom can be clearly seen with two sulfur atoms and two oxygen atoms bonded to phosphorus in Fig. 3. The bond lengths of P1−1 and P1−S2 in SBOB are 2.051 (3) and 1.893 (3) Å, respectively. The bond length of P1−S2 (1.893 (3) Å) is significantly shorter than that of P1−S1 (2.051 (3) Å), that is slightly shorter than those previously reported in the compounds R(S) SP(OC$_6$H$_4$)$_2$ (R = Me, Et or *n*-Pr, the P=S bond length range from 1.899 (2) to 1.913 (2) Å) [25]. Because of formation of S−C bond, the bond length of P1−S1 is

Table 3
The FT-IR spectra data of SBOB.

Wavenumber ($\tilde{\nu}$, cm^{-1})					
(=C−H)	(C=C)	((P)−O−C)	(P−O−(C))	(S−C)	(PS_2)
3030.3 (w), 3057.6 (w).	1461.9 (m), 1508.2 (m), 1596.6 (m)	1152.3 (s), 1208.4 (s), 1242.0 (s)	934.1 (s), 1119.3 (s)	891.3 (m)	698.3 (s), 725.7 (s), 755.2 (m), 475.8 (m), 512.1 (m), 554.0 (m)

Table 5
Crystallographic data of SBOB.

Empirical formula	$C_{27}H_{21}O_2PS_2$
Formula weight	472.53
Temperature (K)	293(2)
Wavelength (Å)	0.71073
Crystal system	Monoclinic
Space group	$P\,2_1/c$
a (Å)	23.5358 (16)
b (Å)	12.2682 (8)
c (Å)	8.1869 (5)
α (°)	90.000
β (°)	95.396 (6)
γ (°)	90.000
V (Å^3)	2353.4 (3)
Z	4
D_{calc} (Mg m^{-3})	1.334
μ (mm^{-1})	0.317
F (0 0 0)	984
Crystal size (mm^3)	0.340 × 0.300 × 0.260
Θ range (°)	3.001–25.008
Index ranges	$-16 \le h \le 27,\ -14 \le k \le 14,\ -9 \le l \le 9$
Reflections collected/unique	9152/4146 (R_{int} = 0.0421)
Completeness (%)	99.7
Data/restraints/parameters	4146/166/379
Goodness of fit on F^2	1.077
Final R indices ($I > 2\sigma(I)$)	R_1 = 0.1066, wR_2 = 0.3077
R indices (all data)	R_1 = 0.1360, wR_2 = 0.3289
Largest diff. peak and hole/(e Å^{-3})	0.448 and −0.498

Table 6
Selected bond distances (Å) and bond angles (°) of SBOB.

S1—P1	2.051 (3)	S2—P1	1.896 (3)
P1—O1	1.598 (6)	P1—O2	1.591 (5)
O1—C1A	1.43 (4)	O1—C1B	1.35 (5)
O2—C11	1.396 (8)	S1—C21	1.824 (10)
C21—S1—P1	99.7 (4)	O2—P1—O1	98.0 (3)
O2—P1—S2	116.4 (2)	O1—P1—S2	117.4 (3)
O2—P1—S1	103.0 (2)	O1—P1—S1	101.0 (2)
S2—P1—S1	117.89 (15)	C1B—O1—P1	123.0 (2)
C1A—O1—P1	128.0 (2)	C11—O2—P1	125.2 (5)

significantly longer than those of the ion compounds $[Et_2NH_2]^+[(4\text{-}MeC_6H_4O)_2P(S)S]^-$ [28], $[Et_3NH]^+[(2\text{-}MeC_6H_4O)_2P(S)S]^-$ [27], $[Et_3NH]^+[(2,5\text{-}Me_2C_6H_3O)_2P(S)S]^-$ [28] and $[Et_3NH]^+[(OCH_2CMe_2CH_2O)P(S)S]^-$ [29]. The S1—P1—S2 bond angle for SBOB is 117.89 (15)°, which is slightly smaller than that in R(S)SP$(OC_6H_4)_2$ (R = Me, Et or *n*-Pr, 118.55 (9)–119.27 (2)°) [25], $[Et_2NH_2]^+[(4\text{-}MeC_6H_4O)_2P(S)S]^-$ (118.68 (7) and 118.61 (7)°) [28], $[Et_3NH]^+[(2\text{-}MeC_6H_4O)_2P(S)S]^-$ (118.62 (4)°) [27], $[Et_3NH]^+[(2,5\text{-}Me_2\ C_6H_3O)_2P(S)S]^-$ (119.06 (5)°) [28] and $[Et_3NH]^+\ [(OCH_2CMe_2CH_2O)P(S)S]^-$ (119.8 (1)°) [29], and significantly smaller than those in $[Et_3NH]^+[CH_2\{6\text{-}t\text{-}Bu\text{-}4\text{-}Me\text{-}C_6H_4O\}_2P(S)S]^-$ (121.03 (9)°) [30]. The O1—P1—O2 bond angle of 98.0 (3)° in SBOB is slightly larger than those in the compounds $[Et_2NH_2]^+[(4\text{-}MeC_6H_4O)_2P(S)S]^-$(96.27 (16) and 96.11 (16)°) [26] and $[Et_3NH]^+[(2\text{-}MeC_6H_4O)_2P(S)S]^-$ (97.07 (8)°) [27], whereas significantly smaller than that in cyclic dithiophosphate salts $[Et_3NH]^+\ [(OCH_2CMe_2CH_2O)\ P(S)S]^-$ (101.4 (2)°) [30] and $[Et_3NH]^+\ [CH_2\{6\text{-}t\text{-}Bu\text{-}4\text{-}Me\text{-}C_6H_4O\}_2P(S)S\ ]^-$ (103.5 (4)°) [30].

Weight loss measurement

Fig. 4 exhibited the effect of SBOB concentration on the inhibition efficiency (η_W, %) for MS in 1.0 M HCl at 303 K. Clearly, the η_W increase with SBOB concentration increasing. With SBOB concentration increase to 80 mg L^{-1} that the η_W change slightly with SBOB concentration further increasing. The growth of η_W is due to the surface coverage of SBOB on MS surface increasing with the concentration increase. The η_W are 95.15% and 97.92%, when SBOB concentration increase to 80 mg L^{-1} and 100 mg L^{-1}, which further demonstrate that SBOB can act as an effective inhibitor.

Potentiodynamic polarization measurement

Fig. 5 presented the polarization curves (Tafel curves) for MS in 1.0 M HCl with various concentrations of SBOB obtained from Tafel curves at 303 K. Meanwhile, the electrochemical parameters including η_T (inhibition efficiency), $I_{c(i)}$ (corrosion current density), $E_{c(i)}$ (vs SCE, V) (corrosion potential), β_c and β_a (cathodic and anodic Tafel slopes) were listed in Table 7.

Based on Fig. 5 and Table 7, it shows that both anodic and cathodic curves shift to lower current densities with adding SBOB in HCl solution, which show that SBOB acting as corrosion inhibitor can reduce the MS corrosion and retard the hydrogen ion (H^+) reduction. The inhibition effect enhances with the increase of SBOB concentration, resulting from the adsorption of SBOB on MS electrode surface. Moreover, from Table 7, the current density is much lower in the presence of SBOB comparing with that in the absence of SBOB in HCl blank solution, and

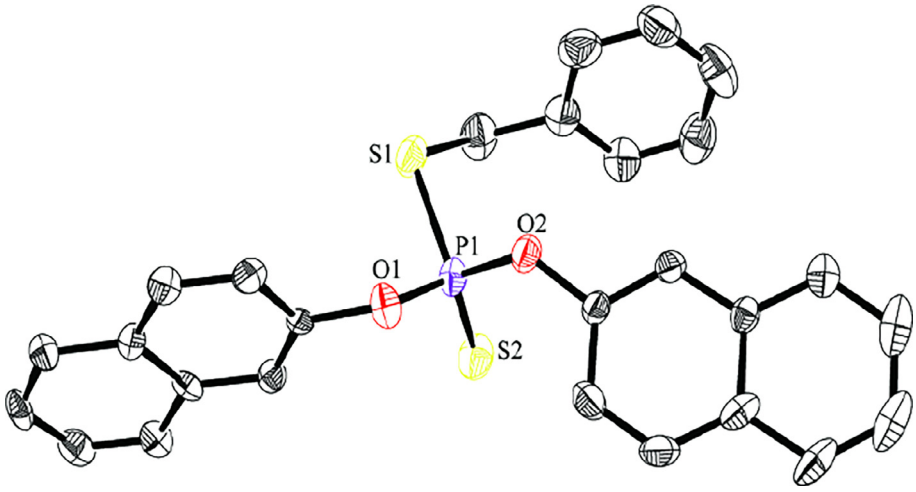

Fig. 3. ORTEP view of SBOB with displacement ellipsoids at the 30% probability level.

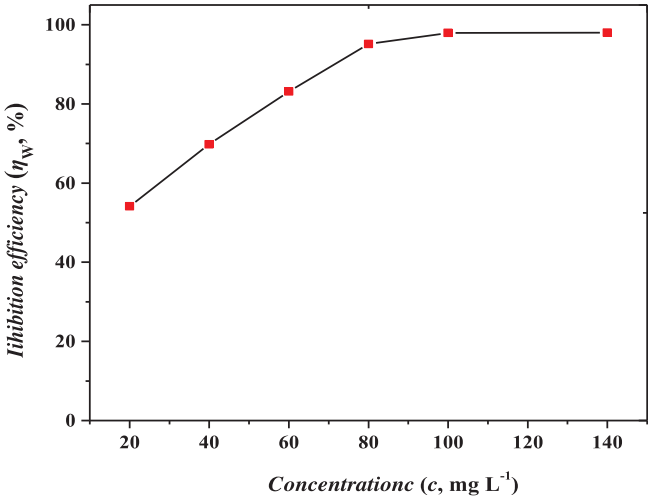

Fig. 4. The effect of SBOB concentration on inhibition efficiency (η_W, %).

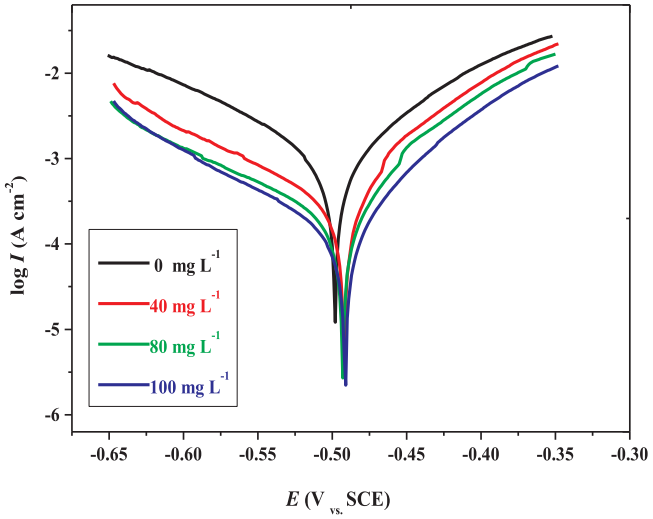

Fig. 5. The Tafel curves of MS in 1.0 M HCl with and without different concentrations of SBOB at 303 K.

which decreases with SBOB concentration increasing. When the concentration of SBOB increases to 100 mg L^{-1}, that η_T will be increased to 95.67%. The result also shows that SBOB can act as effective corrosion inhibitor. Additionally, all corrosion potential for MS corrosion in 1.0 M HCl with different concentration of SBOB at 303 K shifts less than 10 mV (< 85 mV), which shows that SBOB is a mixed-type effective inhibitor [31,32].

Electrochemical impedance spectroscopy

The Nyquist diagrams of MS in 1.0 M HCl with different concentrations SBOB at 303 K from EIS were shown in Fig. 7 according to equivalent circuit mode in Fig. 6. Furthermore, the electrochemical parameters of impedance involving the double layer capacitance (*C*dl), charge transfer resistance (*R*ct) and corresponding inhibition efficiency (η_E, %) obtained from this method were listed in Table 8 in detail.

As shown in Fig. 7, the Nyquist plots show a single capacitive loop, in 1.0 M HCl as the blank solution and aggressive solution with inhibitor (HCl + SBOB), which is attributed to the charge transfer of corrosion process. The impedance spectra show that the single semicircle and the diameter of semicircle increase with SBOB concentration. Moreover, the double layer capacitance decease and charge transfer

Table 7
The polarization parameter and inhibition efficiency (η_T, %) of MS in 1.0 M HCl with and without different concentration of SBOB at 303 K.

c (mg L^{-1})	$E_{c(i)}$ (V)	β_a (mV dec^{-1})	β_c (mV dec^{-1})	$I_{c(i)}$ (μA cm^{-2})	η_T (%)
0	−0.497	131.23	113.25	1970.08	–
40	−0.494	125.79	89.45	588.46	70.13
80	−0.493	123.59	87.41	194.64	90.12
100	−0.491	105.60	81.90	85.30	95.67

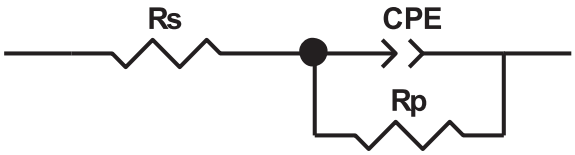

Fig. 6. Equivalent circuit mode.

Table 8
The electrochemical parameters of impedance and corresponding inhibition efficiency (η_E, %) for MS in 1.0 M HCl with and without different concentrations of SBOB at 303 K.

c (mg L^{-1})	R_p (Ω cm^{-2})	C_{dl} (μF cm^{-2})	η_E (%)
0	25.30	77.93	–
40	33.34	56.25	72.44
80	48.95	38.83	88.32
100	62.82	29.23	94.17

resistance increase with SBOB concentration increasing (seen in Table 8). The decrease of double layer capacitance may be due to the decrease of the local dielectric constant or the increase of the thickness of the electrical double layer, indicating that SBOB adsorbed on the MS surface. The increase of charge transfer resistance is resulting from the formation of protective film on the MS/solution interface. The inhibition efficiencies recorded by EIS is 94.17% for MS in 1.0 M HCl with 100 mg L^{-1} SBOB. This result also is in good agreement with the results obtained from weight loss and Tafel measurement.

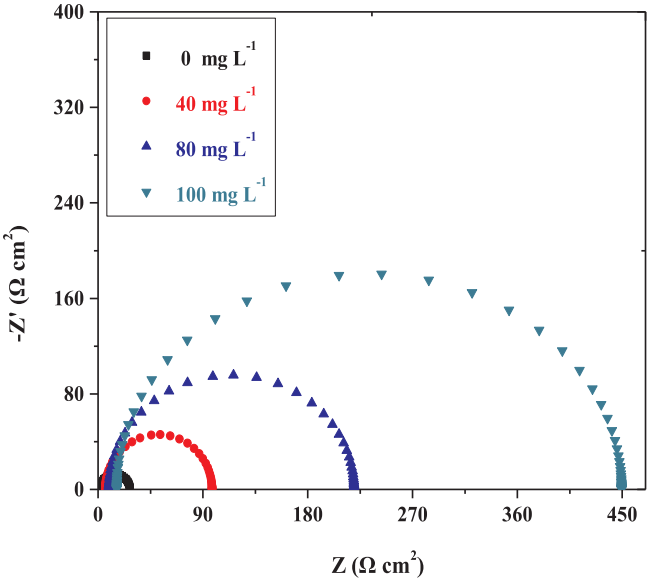

Fig. 7. The Nyquist plots for MS in 1.0 M HCl with and without different concentrations of SBOB at 303 K.

Table 9
Fitting results of different adsorption isotherms for SBOB on MS in 1.0 M HCl at 303 K.

Adsorption isotherms	Pearson's R^2	Equation (y = a + b*x)
Langmuir	0.99082	$y = 0.8531*x + 20.008$
Temkin	0.94107	$y = 0.57711*x - 0.20180$
Freundlich	0.93350	$y = 0.33228*x - 0.68461$
El-Awady	0.89547	$y = 2.17858*x - 2.93134$
Flory–Huggins	0.84804	$y = 0.32159*x - 1.53943$

Adsorption isotherm

According to the data of weight loss measurement from Fig. 4, various isotherms including Langmuir, Frumkin, Flory-Huggins, Al-Awady and Temkin adsorption isotherms are employed to confirm the reasonable adsorption isotherm for SBOB on MS surface in HCl solution. Meanwhile, the fitting results of the five adsorption isotherms for SBOB on MS in 1.0 M HCl were listed in Table 9. Fitting results reveal that the adsorption of SBOB on MS surface obey Langmuir adsorption isotherm showed in Eq. (5) [33,34]. Where c is SBOB concentration, K_A is the

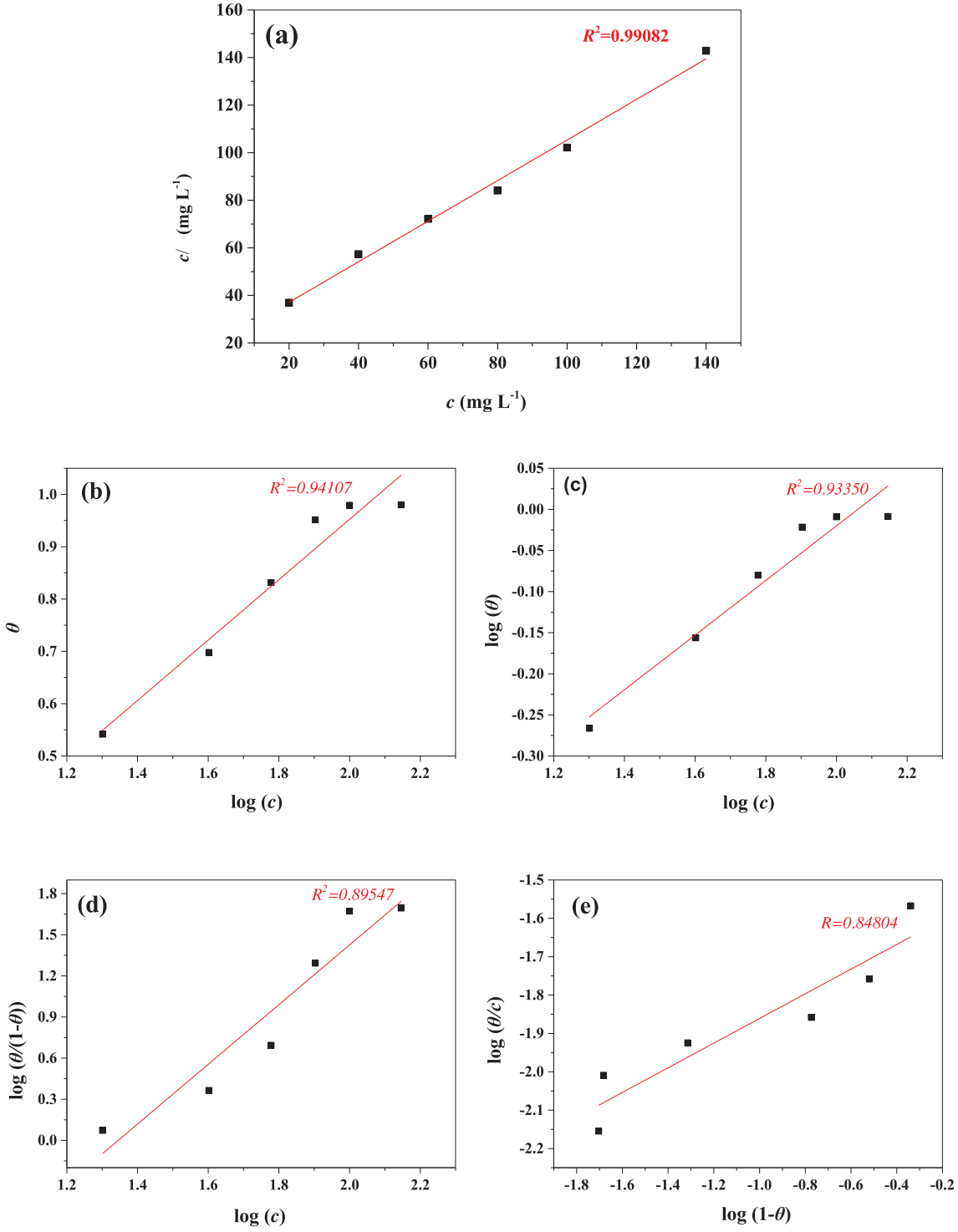

Fig. 8. The plots of Langmuir (a), Temkin (b), Freundlich (c), El-Awady (d) and Flory–Huggins (e) adsorption isotherms for SBOB on MS in 1.0 M HCl at 303 K.

adsorption equilibrium constant and θ is the surface coverage. The surface coverage (θ) for different concentrations of SBOB in 1.0 M HCl is obtained based on Eq. (6) [14,23,32]. In Eq. (6), v_i and v_0 are corrosion rate of the MS in HCl medium with and without different concentrations of SBOB.

$$\frac{c}{\theta} = \frac{1}{K_A} + c \tag{5}$$

$$\theta = \frac{v_0 - v_i}{v_0} \tag{6}$$

Fig. 8(a) shows the plots of c/θ versus c yield the straight lines. While the strong correlation ($R^2 = 0.99082$, see Fig. 8(a)) suggest the adsorption of SBOB on MS surface obeying Langmuir adsorption isotherm. And ΔG^0_{ads} (adsorption standard free energy) can be determined by Eq. (7). The value of intercept ($1/K_A$, in Eq. (5)) = 20.008 (mg L^{-1}), according to this value, the K_{ads} can be calculated using Eq. (8), and the standard free energy of adsorption (ΔG^0_{ads}, kJ mol^{-1} kJ mol^{-1}) can be obtained following Eq. (7), $\Delta G^0_{ads} = -8.314 \times 303.15 \times \ln(55.5 \times 2.364 \times 10^4) = -35.50$ (kJ mol^{-1}). The calculated values of ΔG^0_{ads} for MS corrosion in 1.0 M HCl with different concentrations of SBOB at 303 K is higher than -40.00 kJ mol^{-1}, which is -35.50 kJ mol^{-1}, and it also indicates that the adsorption processes of SBOB on MS surface in 1.0 M HCl belongs to mixed adsorption involving both physisorption and chemisorption [31,35].

$$\Delta G^0_{ads} = -RT\ln(55.5K_{ads}) \tag{7}$$

$$K_{ads} = M_{SBOB} \times K_A \times 10^3 = \frac{473 \times 10^3}{20.008} = 2.364 \times 10^4 (mol\,L^{-1}) \tag{8}$$

Effect factors

The effect of temperature (T, K) on inhibition efficiency (η_W, %) was presented in Fig. 9. It is obvious that with temperature increasing from 298 K to 318 K, the η_W drops from 98.36% to 92.33% for MS in 1.0 M HCl with 100 mg L^{-1} SBOB. The decrease of η_W is due to the increase of desorption for SBOB on MS surface at the higher temperatures [36].

Meanwhile, the effect of HCl concentration (c_{HCl}, M) on η_W at 303 K was shown in Fig. 10. It is obvious that η_W decreases as c_{HCl} increasing, and the η_W of MS corrosion in 0.01 M and 5.0 M HCl with 100 mg L^{-1} SBOB are 99.03% and 60.17%. The decrease of η_W is contributed to the increase of H^+ concentration, and the similar varying tendency was reported by Gou [37].

Additionally, according to the effect of storage time on η_W in Fig. 11, the η_W slightly fluctuates with storage time changing. At 303 K, the η_W in 1.0 M HCl with 100 mg L^{-1} SBOB is still up to 97.44% and 97.33% after 10 and 240 days, respectively. The results show that SBOB can act as the long-acting corrosion inhibitor, which further reveals that SBOB can exhibit the excellent corrosion inhibition. Compared the ionic compounds of N,N-diethylammonium O,O'-di(p-methoxyphenyl)dithiophosphate in our previous work [13,14] with the covalence compound of SBOB, it is evidently seen that the SBOB can stable present in HCl solution.

Quantum chemical study

To explore the correlation between the inhibition performance and molecular structure of SBOB, the quantum chemical calculations were used to investigate the relationships between the inhibition ability and electronic structure of SBOB. Based on this technique, the related quantum chemical results including optimized geometric structure,

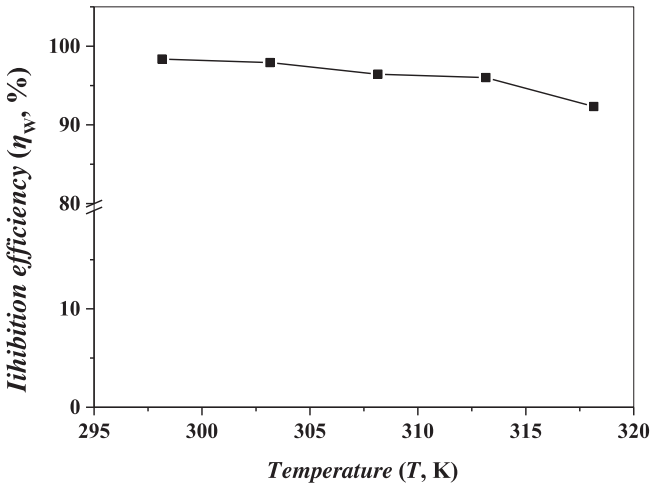

Fig. 9. Effect of temperature (T, K) on inhibition efficiency (η_W, %).

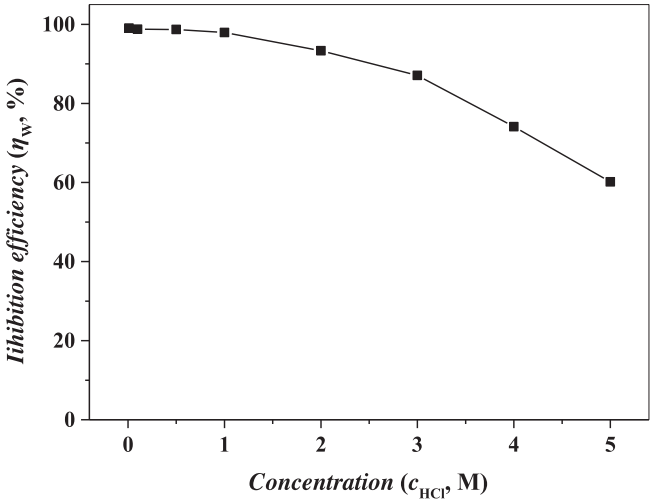

Fig. 10. Effect of HCl concentration (c_{HCl}, M) on inhibition efficiency (η_W, %).

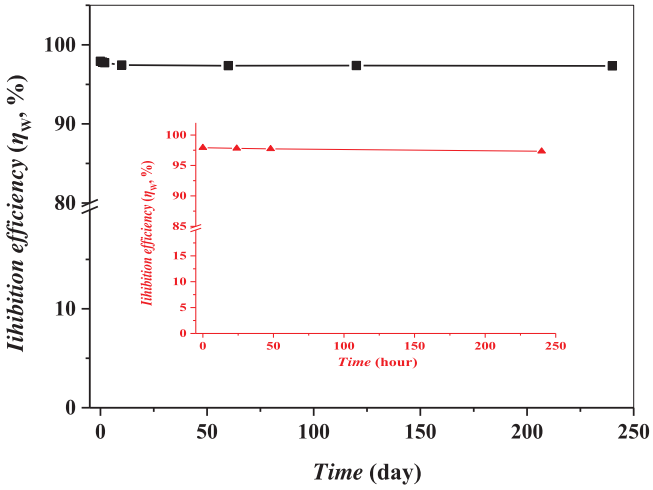

Fig. 11. Effect of storage time on inhibition efficiency (η_W, %).

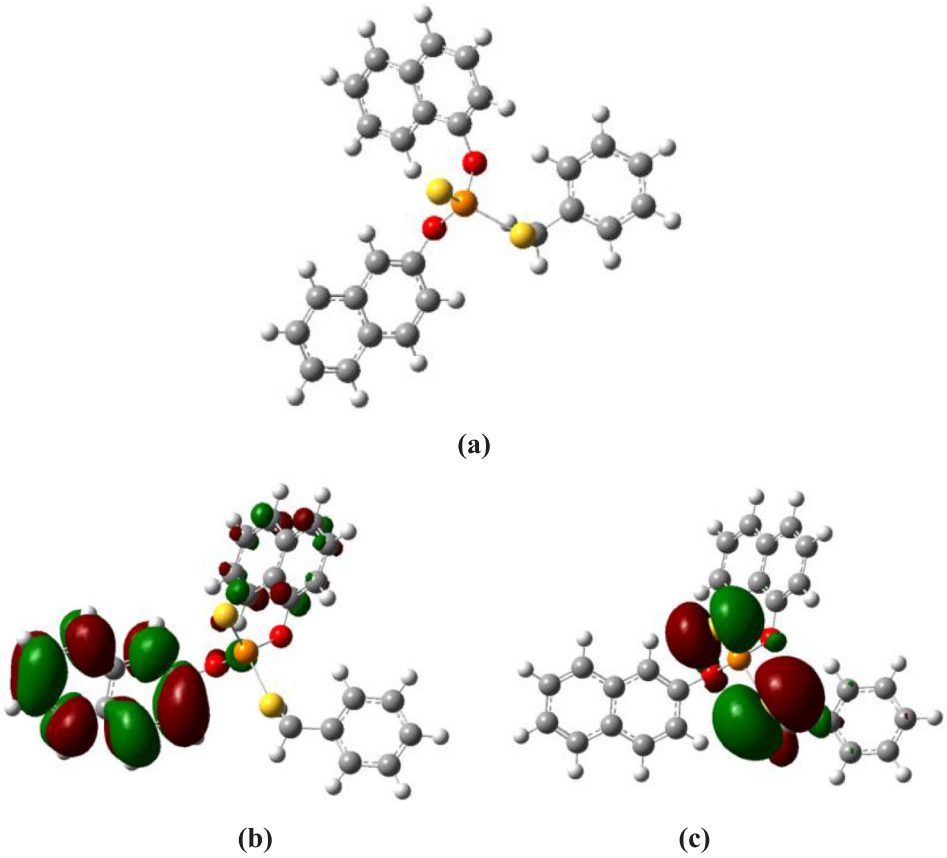

Fig. 12. Optimized molecular structure (a), LUMO orbital (b) and HOMO orbital (c) of SBOB.

Table 10
Quantum chemical parameters for SBOB.

E_{HOMO} (eV)	E_{LUMO} (eV)	ΔE (eV)
−5.878	−2.422	3.456

LUMO and HOMO orbital of SBOB were presented in Fig. 12(a), (b) and (c). Clearly, the electron density distribution of both HOMO and LUMO are localized principally on the sulphur (S) atoms and naphthalene ring, which suggests that the S atoms can be as the active sites for adsorption of SBOB on MS surface. Moreover, the naphthalene ring is a plane conjugated structure, and the inhibitor molecules are likely to take the flat mode adsorbed on MS surface based on the π back bonding. This result is a good confirmation of our previous reports about using dialkyldithiophosphate derivatives as the effective corrosion inhibitor because of the presence of S atoms [38–40].

In addition, the calculated quantum chemical indices including the energy of the lowest unoccupied molecular orbital (E_{LUMO}) and highest occupied molecular orbital (E_{HOMO}), as well as energy gap ($\Delta E = E_{LUMO} - E_{HOMO}$) was listed in Table 10. As a fact, the HOMO and LUMO are often associated with the ability of inhibitor molecule to donate electron and electron-accepting. It is well known that high E_{HOMO} value indicates a strong electron-donating ability to the suitable acceptor, whereas low E_{LUMO} value means the ability of the molecule as an electrons-accepter. From Table 10, the higher value of E_{HOMO} and E_{LUMO} indicates that the SBOB more tends to donate electrons rather than accept electrons. Meanwhile, the ΔE can reflect the stability of the inhibitor molecule, where a smaller ΔE (3.456 eV) implies that SBOB is much easier to be adsorbed on MS surface.

Scanning electron microscopy

The SEM images of MS before and after corrosion in 1.0 M HCl, 1.0 M HCl + SBOB (40 mg L^{-1}) and 1.0 M HCl + SBOB (100 mg L^{-1}) at 303 K for 2.0 h were presented in Fig. 13(a), (b), (c) and (d), respectively. Fig. 13(a) show the SEM images of MS before corrosion, which appears more uniform and some abrading scratches. However, when the MS sample is immersed in blank solution, which is deeply corroded and becomes rough and too uneven displayed in Fig. 13(b), it reveals that the MS surface is highly corroded and damaged in 1.0 M HCl. Furthermore, from Fig. 13(c) and (d), it can be found that the corrosion and dissolution would be suppressed by SBOB in 1.0 M HCl, and it can be concluded that the high performance of inhibitive is due to the adsorbed protective film on MS surface by SBOB.

Conclusions

In conclusion, the new corrosion inhibitor of S-benzyl-O,O'-bis(2-naphthyl)dithiophosphate (SBOB) with ultra-long lifespan was successful synthesized and confirmed by elemental analysis, FT-IR, ^{1}H, ^{13}C, ^{31}P NMR and single crystal X-ray diffraction, respectively. The corrosion inhibition performance was demonstrated by experimental results and quantum chemical calculations analysis. The evaluation of inhibition action shows that the inhibitor of SBOB for mild steel in HCl solution is a mixed-type inhibitor, and the inhibition efficiency decreases with HCl concentration and temperature increasing. However, the corrosion inhibition performance of SBOB keeps almost unchanged after ultra-long storage time. Additionally, the adsorption of SBOB on MS surface obeys Langmuir isotherm.

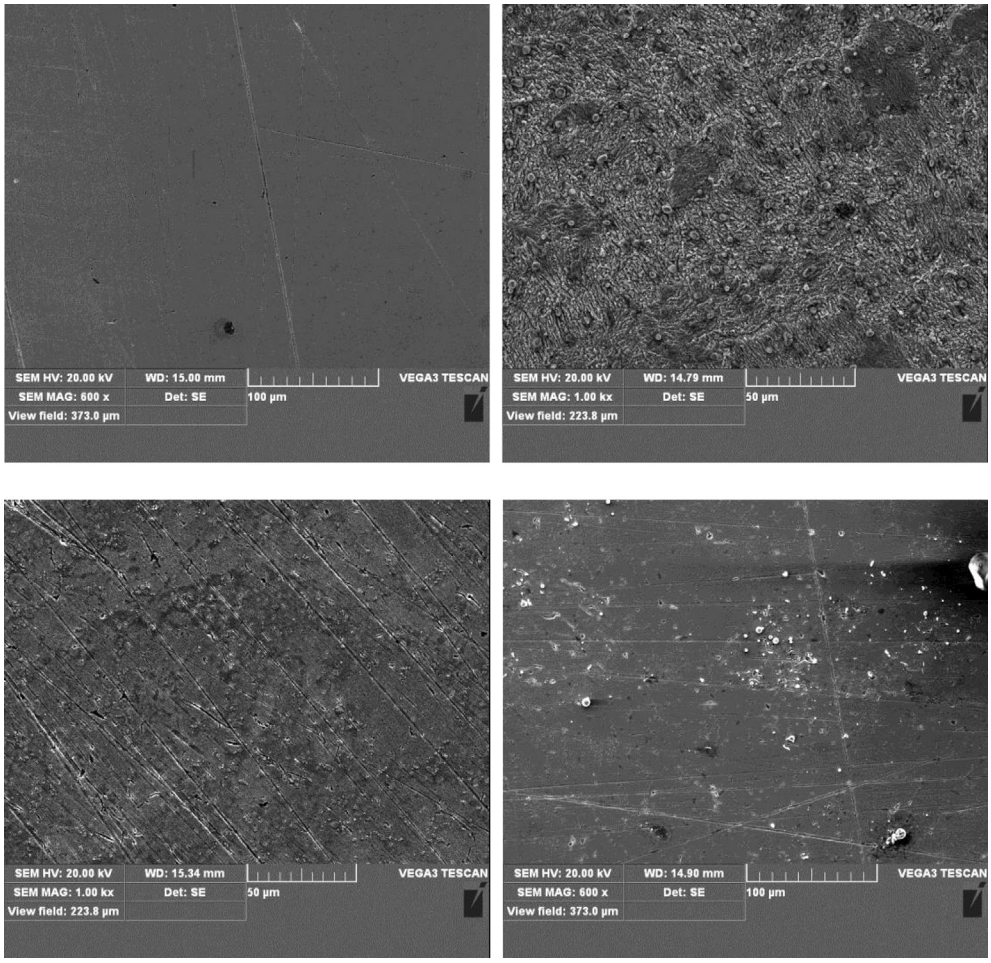

Fig. 13. SEM micrographs of MS before (a) and immersion in 1.0 M HCl (b), HCl + SBOB (40 mg L^{-1}, c) and 1.0 M HCl + SBOB (100 mg L^{-1}, d) at 303 K for 2.0 h.

Acknowledgments

This project is supported financially by the program of Science and Technology Department of Sichuan Province (Nos. 2018JY0061, 2017JY0180), the program of Education Department of Sichuan Province (No. 18CZ0038), the opening project of Material Corrosion and Protection Key Laboratory of Sichuan Province (No. 2017CL02), the opening project of Key Laboratories of Fine Chemicals and Surfactants in Sichuan Provincial Universities (Nos. 2018JXZ01, 2016JXZ03), the opening project of Key Laboratories of Green Catalysis of Higher Education Institutes of Sichuan (No. LZJ1803).

References

[1] Mohan R, Joseph A. Egypt J Petrol 2018;27:11–20.
[2] Al-Azawi KF, Mohammed IM, Al-Baghdadi SB, Salman TA, Issa HA, Al-Amiery AA, Gaaz TS, Kadhum AAH. Res Phys 2018;9:278–83.
[3] Qiang Y, Guo L, Zhang S, Li W, Yu S. J Tan Sci Rep 2016;6:1–14.
[4] Al-Senani GM, Alshabanat M. Int J Electrochem Sci 2018;13:3777–88.
[5] El-Raouf MA, Khamis EA, Kana MTHA, Negm NA. J Mol Liq 2018;255:341–53.
[6] Xhanari K, Finšgar M. RSC Adv 2016;6:62833–57.
[7] Lamaka SV, Vaghefinazari B, Mei D, Petrauskas RP, Höche D, Zheludkevich ML. Corros Sci 2017;128:224–9.
[8] Zhou L, Lv Y, Hu Y, Zhao J, Xia X, Li X. J Mol Liq 2018;249:179–87.
[9] Yildiz R, Döner A, Doğan T, Dehri I. Corros Sci 2014;82:125–32.
[10] Ma X, Jiang X, Xia S, Shan M, Li X, Yu L, Tang Q. Appl Surf Sci 2016;371:248–57.
[11] Ma Q, Qi S, He X, Tang Y, Lu G. Corros Sci 2017;129:91–101.
[12] Zhang K, Xu B, Yang W, Yin X, Liu Y, Chen Y. Corros Sci 2015;90:284–95.
[13] Su X, Lai C, Peng L, Zhu H, Zhou L, Zhang L, Liu X, Zhang W. Int J Electrochem Sci 2016;11:4828–39.
[14] Lai C, Su XL, Jiang T, Zhou LS, Xie B, Li YL, Zou LK. Int J Electrochem Sci 2016;11:9413–23.
[15] Lai C, Guo X, Wei J, Xie B, Zou L, Li X, Chen Z, Wang C. Open Chem 2017;15:263–71.
[16] Lai C, Xie B, Zou L, Zheng X, Ma X, Zhu S. Res Phys 2017;7:3434–43.
[17] Ammal PR, Prajila M, Joseph A. J Environ Chem Eng 2018;6:1072–85.
[18] Han P, Chen C, Li W, Yu H, Xu Y, Ma L, Zheng Y. J Coll Inter Sci 2018;516:398–406.
[19] Mishra A, Verma C, Lgaz H, Srivastava V, Quraishi MA, Ebenso EE. J Mol Liq 2018;251:317–32.
[20] Srivastava M, Tiwari P, Srivastava SK, Kumar A, Ji G, Prakash R. J Mol Liq 2018;254:357–68.
[21] Al-Sabagh AM, El Basiony NM, Sadeek SA, Migaheda MA. Desalination 2018;437:45–58.
[22] Singh A, Ansari KR, Haque J, Dohare P, Lgazd H, Salghi R, Quraishi MA. J Taiwan Inst Chem Eng 2018;82:233–51.
[23] Jiang L, Qiang Y, Lei Z, Wang J, Qin Z, Xiang B. J Mol Liq 2018;255:53–63.
[24] Elemike EE, Nwankwo HU, Onwudiwe DC. J Mol Struct 2018;1155:123–32.
[25] Pérez-García F, Alvarado-Rodríguez JG, Galán-Vidal CA, Páez-Hernández ME, Andrade-López N, Moreno-Esparza R. Struct Chem 2010;21:191–6.
[26] Xie B, Lai C, Xiang Y, Zou L, Xiang Z, Huang C, Yi B. Chin J Appl Chem 2012;29:200–8.
[27] Drake JE, Macdonald CLB, Kumar A, Pandey SK, Ratnani R. J Chem Cryst 2005;35:447–50.
[28] Kour M, Kumar S, Feddag A, Andotra S, Chouaih A, Gupta VK, Kant R, Pandey SK. J Mol Struct 2018;1157:708–15.
[29] Kumar A, Dinesh J, Kour S, Hundal MS, Pandey SK. J Chem Crystallogr 2012;42:299–304.

[30] Swamy KCK, Kumaraswamy S, Raja S, Kumar KS. J Chem Crystallogr 2001;31:51–6.
[31] Cui M, Ren S, Zhao H, Wang L, Xue Q. Appl Surf Sci 2018;443:145–56.
[32] Jiang X, Lai C, Xiang Z, Tang J, Liu L, Tian Gu Y, Wu R, Wu Z, Yuan J, Hou D, Zhang Y. Int J Electrochem Sci 2018;13:6462–72.
[33] Biswas A, Pal S, Udayabhanu G. App. Sur. Sci. 2015;353:173–83.
[34] Fitoz A, Nazır H, Özgür M, Emregül E, Emregül KC. Corro. Sci. 2018;133:451–64.
[35] Fouda1 AS, Etaiw SH, Salah M. Int J Electrochem Sci 2018;13:4670–92.
[36] Lai C, Xie B, Liu C, Gou W, Zhou L, Su X, Zou L. Int. J. Corro 2016;2016:1–8.
[37] Gou W, Lai C, Xiang Z. Int J Electrochem Sci 2017;12:9983–93.
[38] Boucherit L, Douadi T, Chafai N, Al-Noaimi M, Chafaa S. Int J Electrochem Sci 2018;13:3997–4025.
[39] Saqalli L, Galai M, Gharda N, Sahrane M, Ghailane R, Ebn Touhami M, Peres-lucchese Y, Souizi A, Habbadi N. Int J Electrochem Sci 2018;13:5096–119.
[40] Rotaru I, Varvar S, Gaina L, Muresan LM. App. Sur. Sci. 2014;321:188–96.